

ly circulating NNRTI-resistant strains in San Francisco pose a great and immediate threat to global public health.

References and Notes

- B. A. Larder, G. Darby, D. D. Richman, *Science* **243**, 1731 (1989).
- H. M. Truong *et al.*, *AIDS* **20**, 2193 (2006).
- S. M. Blower, H. B. Gershengorn, R. M. Grant, *Science* **287**, 650 (2000).
- J. Goudsmit *et al.*, *AIDS* **15**, 2293 (2001).
- A. Phillips, *Nat. Med.* **7**, 993 (2001).
- E. Tchetgen, E. H. Kaplan, G. H. Friedland, *J. Acquir. Immune Defic. Syndr.* **26**, 118 (2001).
- R. Vardavas, S. Blower, J. J. Miranda, *PLoS ONE* **2**, e152 (2007).
- G. S. Zaric, M. L. Brandeau, A. M. Bayoumi, D. K. Owens, *Simulation* **71**, 262 (1998).
- Materials and methods are available as supporting material on Science Online.
- C. L. Booth, A. M. Geretti, *J. Antimicrob. Chemother.* **59**, 1047 (2007).
- J. Martinez-Picado, M. A. Martínez, *Virus Res.* **134**, 104 (2008).
- L. Ross, N. Parkin, R. Lanier, *AIDS Res. Hum. Retroviruses* **24**, 617 (2008).
- S. Blower, H. Dowlatabadi, *Int. Stat. Rev.* **62**, 229 (1994).
- W. Lang *et al.*, *JAMA* **257**, 326 (1987).
- W. Winkelstein Jr. *et al.*, *JAMA* **257**, 321 (1987).
- J. K. Louie, L. C. Hsu, D. H. Osmond, M. H. Katz, S. K. Schwarcz, *J. Infect. Dis.* **186**, 1023 (2002).
- W. Lang, D. Osmond, K. Page-Bodkin, A. Moss, W. Winkelstein Jr., *J. Acquir. Immune Defic. Syndr.* **6**, 191 (1993).
- W. Lang *et al.*, *J. Acquir. Immune Defic. Syndr.* **4**, 713 (1991).
- J. C. Schmit *et al.*, *AIDS* **12**, 2007 (1998).
- J. J. Eron *et al.*, *N. Engl. J. Med.* **333**, 1662 (1995).
- C. Katlama *et al.*, *JAMA* **276**, 118 (1996).
- D. R. Kuritzkes, *AIDS Patient Care STDS* **18**, 259 (2004).
- B. S. Taylor, M. E. Sobieszczyk, F. E. McCutchan, S. M. Hammer, *N. Engl. J. Med.* **358**, 1590 (2008).
- A. J. Kandathil *et al.*, *Indian J. Med. Microbiol.* **27**, 231 (2009).
- R. M. Granich, C. F. Gilks, C. Dye, K. M. De Cock, B. G. Williams, *Lancet* **373**, 48 (2009).
- L. Breiman, J. H. Freidman, R. A. Olshen, C. J. Stone, *Classification and Regression Trees* (Chapman & Hall, Boca Raton, FL, 1984).
- C. Darwin, *The Origin of Species* (Signet, London, new ed. 1, 2003).
- K. A. Powers, C. Poole, A. E. Pettifor, M. S. Cohen, *Lancet Infect. Dis.* **8**, 553 (2008).
- S. M. Hammer *et al.*, *JAMA* **300**, 555 (2008).
- R.J.S., J.T.O., E.N.B., and S.B. acknowledge the financial support of the National Institute of Allergy and Infectious Diseases (NIAID) (R01 AI041935). R.J.S. is supported by a Natural Sciences and Engineering Research Council of Canada discovery grant, an Early Researcher award, and funding from Mathematics of Information Technology and Complex Systems. In addition, S.B. acknowledges the John Simon Guggenheim Foundation, the National Academies Keck Foundation, and the Semel Institute for Neuroscience & Human Behavior. J.S.K. acknowledges NIAID grants P30-AI27763, NCRK K24RR024369, and AHRQ R18-HS017784. We thank R. Breban, D. Freimer, J. Freimer, N. Jewell, E. Kajita, T. Pytko, V. Supervie, and R. Vardavas for useful discussions throughout the course of this research.

Supporting Online Material

www.sciencemag.org/cgi/content/full/science.1180556/DC1

Materials and Methods

Figs. S1 to S6

Tables S1 to S13

References

13 August 2009; accepted 16 December 2009

Published online 14 January 2010;

10.1126/science.1180556

Include this information when citing this paper.

Optimal Localization by Pointing Off Axis

Yossi Yovel,¹ Ben Falk,² Cynthia F. Moss,² Nachum Ulanovsky^{1*}

Is centering a stimulus in the field of view an optimal strategy to localize and track it? We demonstrated, through experimental and computational studies, that the answer is no. We trained echolocating Egyptian fruit bats to localize a target in complete darkness, and we measured the directional aim of their sonar clicks. The bats did not center the sonar beam on the target, but instead pointed it off axis, accurately directing the maximum slope (“edge”) of the beam onto the target. Information-theoretic calculations showed that using the maximum slope is optimal for localizing the target, at the cost of detection. We propose that the tradeoff between detection (optimized at stimulus peak) and localization (optimized at maximum slope) is fundamental to spatial localization and tracking accomplished through hearing, olfaction, and vision.

Most sensory systems allow some active control over the information acquired from the environment (1–6). Nowhere is this more evident than in echolocating bats (4, 7–10), which control many aspects of their sonar signal design (4, 7, 9, 11–16) and use returning echoes to orient and forage in the dark (4, 7–16). We trained Egyptian fruit bats to fly in a large flight room and land on a spherical target while relying exclusively on sonar (17). The bats’ three-dimensional (3D) position was measured with two infrared cameras, and the shape and direction of their sonar beam pattern were measured with a 20-microphone array (17) (Fig. 1, A to D, and movie S1).

At the beginning of each trial, the target was randomly repositioned. Subsequently, the bat

sought for the target, approached it, and landed on it, either by a straight flight or a curved trajectory (Fig. 1C and fig. S1). Unlike microbats (microchiropteran bats), which emit laryngeal tonal calls, Egyptian fruit bats are megabats (megachiropteran bats) that produce very short (50- to 100- μ s) impulse-like tongue clicks, with frequencies centered at 30 to 35 kHz (fig. S2). While flying, bats typically emitted pairs of clicks, with an \sim 20-ms interval within the click pair and an \sim 100-ms interval between the pairs (Fig. 1A and fig. S3) (18, 19). The bats pointed their sonar beam toward the left or the right, in an alternating manner as follows: left \rightarrow right \rightarrow 100-ms interval \rightarrow right \rightarrow left (Fig. 1D and movie S1).

We observed two different phases of behavior. During the first stage, the bats did not necessarily lock their click pairs onto the target, and the directions of clicks were widely distributed (the “unlocked” phase). At the final stage, the bats directed their sonar clicks so that the vector average of the pair of clicks pointed toward the target with accuracy better than 30°

(17). We refer to this as the “locked” phase (Figs. 1E, arrows, and 2A, top, and fig. S1C). During this phase, 0.5 s before landing, 80% of the click pairs were locked with accuracy better than 15° (Fig. 2A, bottom, gray lines). In 10% of the trials, the bats locked onto the target with average accuracy better than 5°. The left-right orientation of the clicks in the locked phase implies that the bats did not direct the maximum intensity of the click toward the target, contradicting the common notion that bats steer their sonar beam in order to maximize the signal-to-noise ratio (SNR) of the echoes (13, 20).

Another possible strategy would be for the bats to direct the maximal slope of the beam’s emission curve toward the target, because this would maximize changes in reflected echo energy that result from changes in the relative position of the bat and the target. Plotting the directional span of the beams between the right and left maximum slope (green lines in Fig. 1, E and F, and fig. S1, C and D) showed that the bats consistently placed the maximum slope of their beams onto the target (Fig. 1F and fig. S1D; the top and bottom of the green lines are close to direction 0°). Next, we examined the population distribution of the directions of the beams’ maximum intensity and maximum slope (Fig. 2, B and C, top two rows). Before locking, the bats directed their sonar beams over a wide range of angles, spanning $>100^\circ$ around the target (Fig. 2B, top). After locking, however, they clearly directed their beam so that the maximum slope of the intensity curve of the beam, and not its peak, was on the target (Fig. 2C, middle row). All six bats exhibited this behavior (fig. S4).

When the maximum slope of the beam is directed toward an object, any motion of the object relative to the bat will result in the largest possible change in echo intensity. The sign of the energy change (positive or negative) corresponds to the

¹Department of Neurobiology, Weizmann Institute of Science, Rehovot 76100, Israel. ²Department of Psychology, Institute for Systems Research and Neuroscience and Cognitive Science Program, University of Maryland, College Park, MD 20742, USA.

*To whom correspondence should be addressed. E-mail: nachum.ulanovsky@weizmann.ac.il

direction of motion. We hypothesized that Egyptian fruit bats lock the maximum slope on the target as a strategy that maximizes their sensitivity to changes in target azimuth, in order to better localize the target.

To test this “optimal-localization” hypothesis, we used the Fisher information (FI) measure that is commonly used to assess sensitivity to small differences (21). To estimate the FI at different angles relative to the target, we computed joint probability-density functions of the intensities and angles for all clicks (17). After locking, the beam-steering strategy used by the bats maximized the FI in the direction of the target (Fig. 2C, bottom row). There is a secondary peak in the FI curve, because each emission curve has two points of maximum slope (one on each side). The secondary peak is higher because of the inherent asymmetry of the beam (Fig. 3A). Because the FI is a measure that meets a theoretical optimality criterion (21), this result implies that the strategy used by the bats is optimal for localizing the target based on the intensity of reflected echoes.

We ruled out an alternative explanation for the bats’ behavior, namely that they might have placed the peaks of the beams on the target’s edges. In this case, we would expect the angle between the pair of clicks to increase as the bat approaches the target, because the angular extent of the target increases. However, we found no such increase in angle (fig. S5).

This optimal-localization strategy is not free of cost. When pointing the maximum slope of the emission curve and not its peak toward an object, less energy (6 dB) is reflected back from the object (Fig. 3, A and B), and this reduces object detectability, decreasing the maximal detection range by ~16% (17). We hypothesize, therefore, that the part of the beam between the peak and the maximum slope of the emission curve can be used by bats to trade off between detection and localization. The beam’s peak provides optimal detection, whereas the maximum slope provides optimal localization. The bat could direct the beam according to the task, target properties, or ambient noise. Bats landing on an acoustically salient object, as in our experiments, preferred to maximize spatial localization in order to land accurately. A bat confronted by a detection problem, such as a small target, a noisy environment, or a strong masker, should act to maximize detection by placing the beam’s peak on the target (22). A bat that needs both detection and localization will have to compromise between the two positions on the emission curve (Fig. 3B). Indeed, the area between the peak and the slope was directed toward the target more often than the area beyond the slope, which is consistent with a detection-localization compromise [Fig. 2C, top; the peak’s distributions are significantly skewed toward the target at angle 0°; *t* test: $\gamma_{\text{right}} = -0.42$, $P < 0.001$; $\gamma_{\text{left}} = 0.26$, $P < 0.001$ (17)].

To further test this “detection-localization tradeoff” hypothesis, we conducted a control experiment in which a large reflecting board was positioned 50 to 80 cm behind the target (17). Such a reflector returns strong echoes that arrive shortly after the target’s echo, thus acting as a powerful acoustic masker that interferes with target detection. Indeed, some bats changed their beam-steering strategy; initially they maintained the left→right→right→left pattern as described above, but then, in the final approach (~1 s before landing), they directed both clicks of each click pair forward and pointed at the target a part of the emission curve that was close to the beam’s peak (Fig. 3C, bottom, black dots, and fig. S6). This switch in strategy was exhibited by bats that chose to fly directly toward the target. It should increase echo energy and improve detection (improve SNR). The bats’ flexibility in steering their emission beams suggests that in our main experiments (Figs. 1 and 2), the animals actively chose to direct the maximum slope of the beam toward the target.

It remains an open question whether other echolocating animals (microbats, dolphins, swiftlets, etc.) use the maximum-slope strategy for localizing objects. All studies that tested beam steering in microbats (13, 20, 23) did so in the context of small targets, which created a detection problem. We predict that, when localization is paramount and detection is not challenged, microbats would also use the slope-based optimal-localization

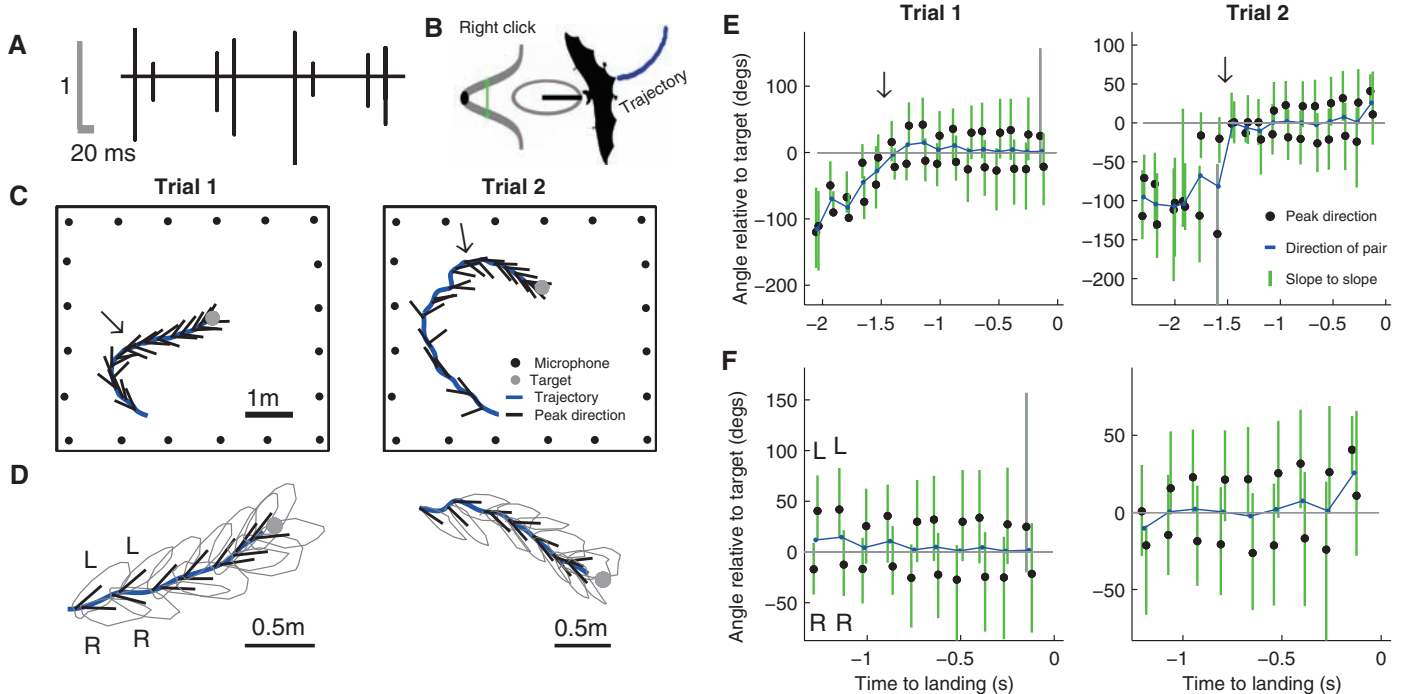


Fig. 1. Examples of flight and echolocation behavior. (A) Representative time signal showing four click pairs. The y axis shows signal amplitude (on a linear scale, with the largest excursion normalized to 1). (B) Schematic of bat emitting a right click. Ellipse, sonar beam in polar coordinates; Gaussian curve, sonar beam in Cartesian coordinates; black dot, peak intensity. The green line connects the two points of maximum slope. (C to F) Examples of two behavioral trials. (C) Top view of the room. Blue line, bat’s flight trajectory; short black lines, sonar beam directions for all clicks; arrow, point of

locking onto target. (D) Close-up on locked part of the trials in (C); same notation as in (C). Gray curves, polar representation of the beams (dB scale). (E) Diagrams of beam angles relative to the target for the same two trials. Green lines connect the beam’s right and left maximum slope. Gray lines, clicks that did not meet the inclusion criteria (17); black dots, direction of beam’s peak; blue line, average direction of each pair of black dots; arrows, point of locking. (F) Close-up on the locked part of (E); same notation as in (E). The bats tended to place the maximum slope (end of green lines) onto the target.

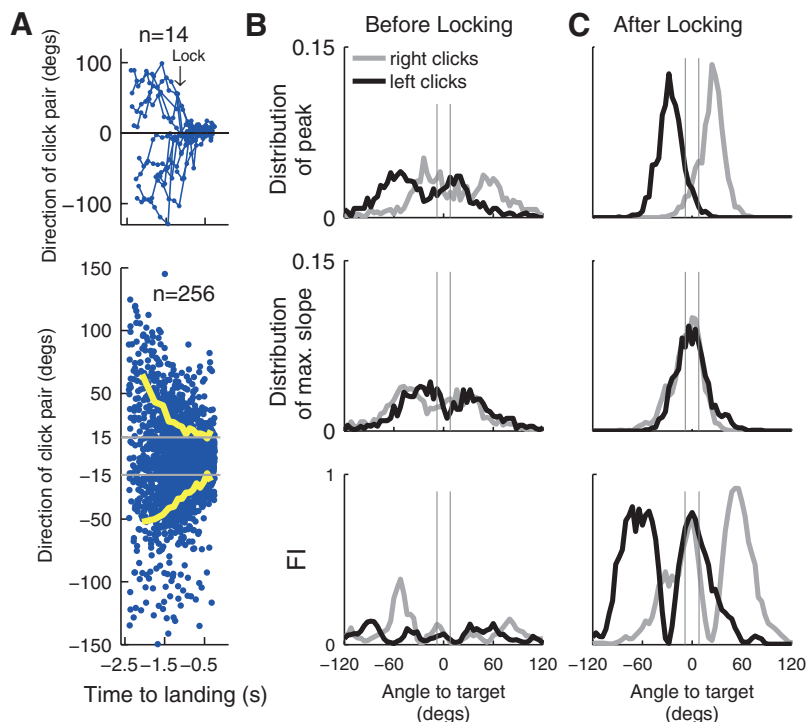
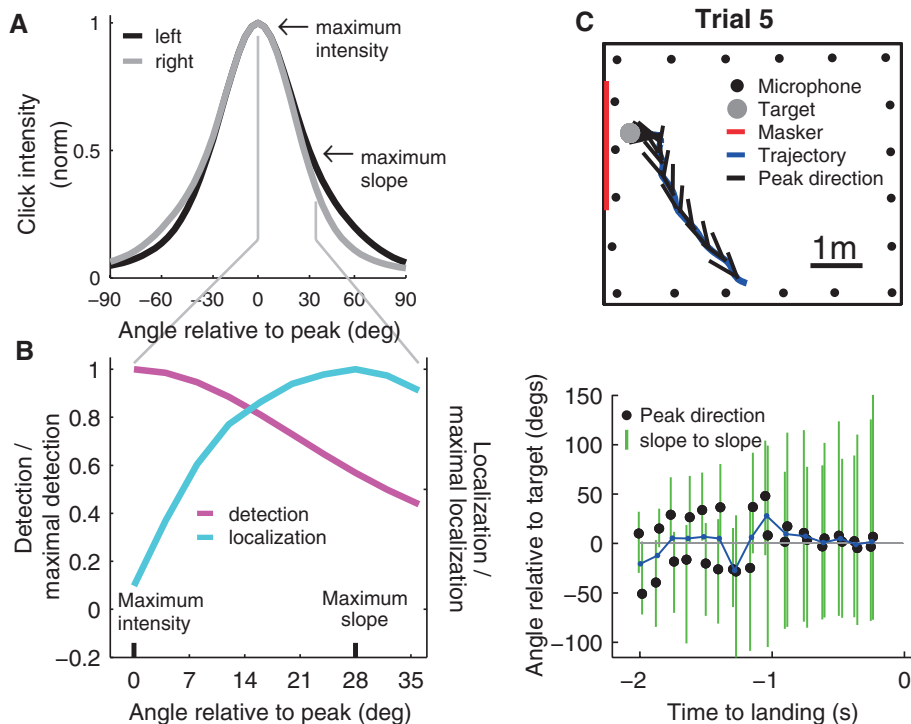


Fig. 2. Population analysis shows that bats optimize angular localization by locking the maximum slope of the beam onto the target. **(A)** Top: Direction of click pair (vector average) relative to the target as function of time to landing for 14 example trials. Blue lines, same notation as blue lines in Fig. 1E; black arrow, average time of locking onto target. Bottom: The same for all 256 trials. Yellow lines, mean \pm SD, computed in 100-ms windows; gray lines, $\pm 15^\circ$. **(B and C)** Directional distributions of click parameters and FI relative to target direction, **(B)** before locking and **(C)** after locking. Top: distribution of the direction of the beam's peak intensity. Middle: distribution of the direction of the beam's maximum slope. Bottom: FI as function of angle to target. Gray vertical lines, $\pm 5.5^\circ$ total error in estimating bat/object directions (17). The y axes are identical in **(B)** and **(C)**.

Fig. 3. The tradeoff between detection and angular localization. **(A)** Average left click and right click (averaged across all locked clicks of all bats). The emission curve is asymmetric (less steep on the side directed toward the target). This explains the higher secondary peaks in the FI curve (Fig. 2C, bottom). **(B)** Detection-localization tradeoff for the biosonar of Egyptian fruit bats. Magenta, detection (in normalized units); cyan, localization (azimuthal discriminability, d'). The x axis shows the angle within the emission beam, shown between the peak and 36° . The localization accuracy decreases beyond the maximum slope. **(C)** Example of flight trajectory and echolocation behavior for one trial from the masker experiments (detection problem). Top and bottom, same notations as in Fig. 1, C and E, respectively; red line, masker. Approximately 1 s before landing, the bat switched from a left-right maximum-slope strategy to a peak strategy (black dots).

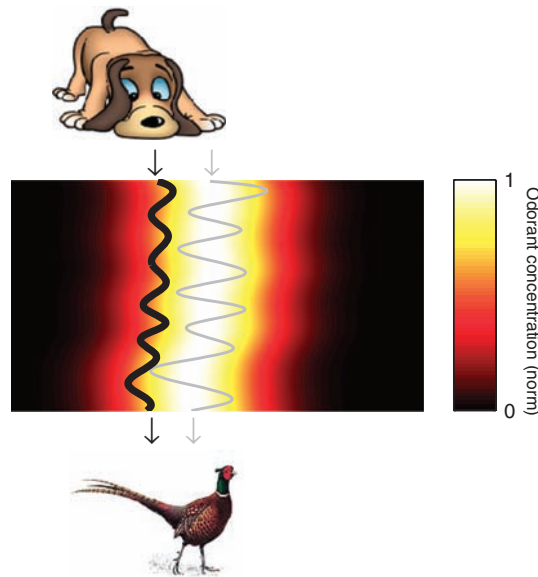


strategy; however, because microbat biosonar is based on single pulses instead of double clicks (4, 7–10), the microbats would always place one of the beam's slopes on target (for example, right→right→right...) and analyze echo-amplitude changes between successive calls. The mechanism by which Egyptian fruit bats direct their beams left→right is not entirely clear [supporting online material (SOM) text], but the alternating clicks of these megabats are certainly advantageous in that comparing two different slopes doubles the intensity difference.

Previous neurophysiological studies in microbats have reported auditory neurons tuned to echo amplitude (24). Our results point to the possibility that, in megabats, upstream of such echo-amplitude-tuned neurons, there might be neurons that are sensitive to the amplitude difference of two successive echoes (20 ms apart). In both microbats and megabats, the directional accuracy of passive hearing is 10° to 15° (25), whereas active mechanisms, such as described here, could underlie the improved accuracy of 1.5° to 5° during active echolocation (12, 20).

We further hypothesize that the tradeoff between detection (SNR) and localization is a general dilemma in sensory systems. If we describe the intensity of a stimulus (for example, olfactory or visual) as a contour in space, its peak would be optimal for detection, but the maximum slope is optimal for spatial localization. For example, we predict that an organism following an odor trail should follow the line of the maximum slope of the odor concentration in order to optimize the tracking accuracy and minimize movement jitter (Fig. 4). A study that measured odorant spatial distribution in an

Fig. 4. Prediction for other sensory systems (olfaction). Color map, schematic odor trail; gray line, path of an organism that followed the trail's peak concentration. This strategy is typically assumed for odor-trail following (3). Black line, path of the same organism when using a strategy similar to that of our bats, that is, following the maximum slope of the odorant concentration (17). The movement jitter in this case is smaller, making the tracking smoother and therefore faster.



olfactory-tracking task indicated that *Drosophila* larvae seem to follow a trajectory between the peak and the maximum slope (26). Similarly, in the case of vision, we predict that when tracking large moving objects, humans would place their fovea on the object's intensity slope to optimize tracking. Finally, several recent studies have reported sensory neurons that best encode stimulus location via the maximum slope of their tuning curve (22, 27–29), not via the peak firing rate of the tuning curve. Such coding maximizes the discriminability of the on-slope stimulus, paralleling our behavioral results, which show an optimal-localization strategy at the sensor's behavioral level.

References and Notes

1. D. Kleinfeld, E. Ahissar, M. E. Diamond, *Curr. Opin. Neurobiol.* **16**, 435 (2006).
2. K. C. Catania, *Nature* **444**, 1024 (2006).
3. J. Porter *et al.*, *Nat. Neurosci.* **10**, 27 (2007).
4. N. Ulanovsky, C. F. Moss, *Proc. Natl. Acad. Sci. U.S.A.* **105**, 8491 (2008).
5. M. E. Nelson, M. A. MacIver, *J. Comp. Physiol. A* **192**, 573 (2006).
6. W. W. Au, K. J. Benoit-Bird, *Nature* **423**, 861 (2003).
7. G. Jones, M. W. Holderied, *Proc. Biol. Sci.* **274**, 905 (2007).
8. H.-U. Schnitzler, C. F. Moss, A. Denzinger, *Trends Ecol. Evol.* **18**, 386 (2003).
9. J. A. Simmons, M. B. Fenton, M. J. O'Farrell, *Science* **203**, 16 (1979).
10. N. Suga, *J. Exp. Biol.* **146**, 277 (1989).
11. W. Metzner, *Nature* **341**, 529 (1989).
12. W. M. Masters, A. J. Moffat, J. A. Simmons, *Science* **228**, 1331 (1985).

13. K. Ghose, C. F. Moss, *J. Neurosci.* **26**, 1704 (2006).
14. N. Ulanovsky, M. B. Fenton, A. Tsoar, C. Korine, *Proc. Biol. Sci.* **271**, 1467 (2004).
15. C. Chiu, W. Xian, C. F. Moss, *Proc. Natl. Acad. Sci. U.S.A.* **105**, 13116 (2008).
16. E. K. V. Kalko, H.-U. Schnitzler, *Behav. Ecol. Sociobiol.* **33**, 415 (1993).
17. Materials and methods are available as supporting material on Science Online.
18. R. A. Holland, D. A. Waters, J. M. Rayner, *J. Exp. Biol.* **207**, 4361 (2004).
19. H. V. Herbert, *Z. Säugetierkd.* **50**, 141 (1985).
20. K. Ghose, C. F. Moss, *J. Acoust. Soc. Am.* **114**, 1120 (2003).
21. P. Dayan, L. F. Abbott, *Theoretical Neuroscience* (MIT Press, Cambridge, MA, 2001).
22. D. A. Butts, M. S. Goldman, *PLoS Biol.* **4**, e92 (2006).
23. A. Surlykke, K. Ghose, C. F. Moss, *J. Exp. Biol.* **212**, 1011 (2009).
24. T. Manabe, N. Suga, *J. Ostwald, Science* **200**, 339 (1978).
25. R. S. Heffner, G. Koay, H. E. Heffner, *J. Comp. Psychol.* **113**, 297 (1999).
26. M. Louis, T. Huber, R. Benton, T. P. Sakmar, L. B. Vosshall, *Nat. Neurosci.* **11**, 187 (2008).
27. N. S. Harper, D. McAlpine, *Nature* **430**, 682 (2004).
28. A. Brand, O. Behrend, T. Marquardt, D. McAlpine, B. Grothe, *Nature* **417**, 543 (2002).
29. D. McAlpine, D. Jiang, A. R. Palmer, *Nat. Neurosci.* **4**, 396 (2001).
30. We thank N. Sobel, J. Rubin, E. Simoni, A. Rubin, and N. Harper for comments on the manuscript; M. Holderied, I. Couzin, A. Arieli, E. Ahissar, and H.-U. Schnitzler for helpful discussions; and J. Barcelo for technical assistance. This study was funded by a Human Frontiers Science Program grant to N.U. and a Weizmann Institute Postdoctoral Fellowship to Y.Y.

Supporting Online Material

www.sciencemag.org/cgi/content/full/327/5966/701/DC1

Materials and Methods

SOM Text

Figs. S1 to S7

Movie S1

References

14 October 2009; accepted 23 December 2009

10.1126/science.1183310

Axon Extension Occurs Independently of Centrosomal Microtubule Nucleation

Michael Stiess,¹ Nicola Maghelli,² Lukas C. Kapitein,³ Susana Gomis-Rüth,¹ Michaela Wilsch-Bräuninger,² Casper C. Hoogenraad,³ Iva M. Tolić-Nørrelykke,² Frank Bradke^{1*}

Microtubules are polymeric protein structures and components of the cytoskeleton. Their dynamic polymerization is important for diverse cellular functions. The centrosome is the classical site of microtubule nucleation and is thought to be essential for axon growth and neuronal differentiation—processes that require microtubule assembly. We found that the centrosome loses its function as a microtubule organizing center during development of rodent hippocampal neurons. Axons still extended and regenerated through acentrosomal microtubule nucleation, and axons continued to grow after laser ablation of the centrosome in early neuronal development. Thus, decentralized microtubule assembly enables axon extension and regeneration, and, after axon initiation, acentrosomal microtubule nucleation arranges the cytoskeleton, which is the source of the sophisticated morphology of neurons.

The centrosome is regarded as the primary source of microtubules in axonal and dendritic growth (1, 2). It is thought that microtubules assemble at the centrosome, then are released and move along the axon through motor

proteins (1, 3, 4). Furthermore, in vitro the centrosome directs axon formation in vertebrate and invertebrate neurons (5, 6), but this has not been confirmed in vivo (7). Microtubules, however, can also assemble locally from subunits or

small oligomers within the axon (8–10). Indeed, flies that lose centrosomes during development seem to develop a largely normal nervous system, where the direction of axon outgrowth appears not to be affected (11). Thus, the role of the centrosome and centrosomal microtubule nucleation in axon growth is controversial (12–15).

To define the role of the centrosome in microtubule nucleation during neuronal development, we first determined where microtubules are nucleated during the development of rodent hippocampal neurons. Microtubules were depolymerized with nocodazole, and the microtubule nucleation sites were examined after washout of the drug (Fig. 1A). In young neurons that had just initiated an axon [2 days in vitro (DIV)], microtubules

¹Independent Junior Research Group Axonal Growth and Regeneration, Max Planck Institute of Neurobiology, Am Klopferspitz 18, 82152 Martinsried, Germany. ²Max Planck Institute of Molecular Cell Biology and Genetics, Pflotenhauerstrasse 108, 01307 Dresden, Germany. ³Department of Neuroscience, Erasmus Medical Center, Dr. Molewaterplein 50, 3015 GE Rotterdam, Netherlands.

*To whom correspondence should be addressed. E-mail: fbradke@neuro.mpg.de



Supporting Online Material for **Optimal Localization by Pointing Off Axis**

Yossi Yovel, Ben Falk, Cynthia F. Moss, Nachum Ulanovsky*

*To whom correspondence should be addressed. E-mail: nachum.ulanovsky@weizmann.ac.il

Published 5 February 2010, *Science* **327**, 7010 (2010)
DOI: 10.1126/science.1183310

This PDF file includes:

Materials and Methods

SOM Text

Figs. S1 to S7

References

Other Supporting Online Material for this manuscript includes the following: (available at www.sciencemag.org/cgi/content/full/327/5966/701/DC1)

Movie S1

Materials and Methods

Animals and training: Six adult Egyptian fruit bats (*Rousettus aegyptiacus*) were trained to detect, localize, approach and land on a large sphere (10-cm diameter) that was mounted on a vertical pole positioned inside a large flight-room ($6.4 \times 6.4 \times 2.7$ m). These bats typically use their echolocation in order to land on fruits, and for general orientation in the environment; the target's size was similar to some fruits eaten by these bats, such as mango. The walls and ceiling of the room were covered with acoustic foam and the pole was covered with felt, to minimize reverberations; in contrast, the target sphere was made of an acoustically highly-reflective material (Polystyrene), in order to make it the most salient acoustically-reflective object in the flight room. We used several steps to ensure that the bats were relying solely on echolocation to perform the task: (i) The target was painted black and the room was in complete darkness (illuminance $< 10^{-4}$ lux), to exclude the possibility of using visual cues. The experimenter, who was inside the room, wore night-vision-goggles with infrared illumination. (ii) The bats were food-rewarded only after landing on the target, to prevent use of olfactory cues; the target was cleaned with soap and water after every three trials to remove any possible odors that remained on it due to the contact with the bat. (iii) After every trial, the target was randomly re-positioned inside the room, both in the horizontal and in the vertical direction (the pole had a telescopic mechanism that allowed changing the target height). The bats needed ~ 4 weeks in order to learn the task, and once they learned it they always succeeded in landing on the target. All experimental procedures were approved by the Institutional Animal Care and Use Committees of the Weizmann Institute of Science and the University of Maryland.

Sound recordings: The bats' echolocation behavior was recorded with an array of 20 microphones, which were spaced 1-m from each other around a rectangular supporting frame (5.3×5.2 m, Fig. 1C, rectangle), at a height of 90 cm above the floor (Fig. 1C, black circles). The dynamic range of the microphones, which we measured by playing synthetic sounds, was > 30 dB, and the noise level of the microphones was < 0.1 dB; this large dynamic range and low noise level allowed a high-fidelity measurement of the bat's sonar clicks on multiple microphones. The signal from each microphone was amplified and fed into a band-pass filter centered around 35 kHz, with a frequency response that fits very well the frequency content of the Egyptian fruit bat's sonar click (fig. S2). Next, the signal was fed to an electronic circuit which extracted the envelope of this band-passed signal. The envelope was then low-pass filtered (prolonging each click to ~ 250 - μ s duration) and digitized into a data-acquisition computer. Each microphone channel was sampled at 20 kHz. Finally, the signal was translated into a dB scale in which analysis was performed. In 20 trials the audio was also recorded using 3 wideband ultrasonic microphones positioned on the floor (sampled at 250 kHz/channel): These recordings enabled us to analyze the clicks' spectra (fig. S2).

Video recording: Two infrared digital video cameras running at 125 Hz were used to record the flight of the bats. The direct-linear-transform algorithm was used to measure the locations of the bat and other objects from the two camera views, and compute their three-dimensional location coordinates (1, 2). Video and sound were both recorded in segments of 16 seconds (recording was manually triggered). The cumulative drift between the clocks of the audio and videos systems over an entire recording trial was < 1 ms.

General behavior: Once the target was randomly positioned in the room (after the previous trial), the trained bat typically started echolocating while hanging on the wall. It would then fly towards the target, but usually did not land on it in the first attempt, but rather passed it and landed on the wall. After a short pause the bat typically flew again towards the target, approaching it either directly or in a curved path, landed on it and waited for the reward (a piece of banana). When approaching the target, the bats did not increase substantially the pulse repetition rate as is usually done by microbats, probably because the Egyptian fruit bats were already operating at their maximal click-rate. Once rewarded, the bats usually flew away with the reward, hung on one of the walls and ate it there. Eating and resting normally lasted >1 minute, during which the bat did not echolocate. Thus, the bat would start echolocating only after the target was already re-positioned to its new location.

Reconstruction of the beam shape: The signals from each microphone were segmented to include vocalizations and exclude echoes. The intensity of each microphone was corrected for spherical loss and atmospheric attenuation, using the measured position of the bat and the values of the room temperature and humidity (1, 2). The 20 intensity values from the 20 microphones were first smoothed using a 3rd-degree Golay-Savitzky filter, and were then used to reconstruct a horizontal cross-section of the beam. The average angular resolution of the raw recorded beam was $\sim 15^\circ$. Because the beam shape is smooth, we first interpolated the beam linearly so the maximum angular distance between two intensity values was 20° , and then interpolated the resulting beam using a polynomial cubic spline to create an equal azimuthal spacing of 4° . The accuracy of the video tracking was estimated to be $\sim 4^\circ$ (this estimate was done by re-tracking 5 trials $5\times$ times each and computing the s.d.).

The total weighted error in computing the azimuthal angles of objects in the room relative to the bat – taking into account the 4° errors of both the video and sound systems and using the propagation of errors formula – is therefore $\sqrt{4^2 + 4^2} \sim 5.5^\circ$; this error is denoted by the vertical gray lines in Fig. 2B,C. We also conducted a separate analysis which showed that the horizontal cross-sectioning of the beam, as "cut" by the microphone-array, does not change any of the results (fig. S7).

Inclusion criteria for sonar clicks: To ensure that we were only using high-quality data, we included in the analyses of Fig. 2 (histograms and Fisher information) only clicks that met the following inclusion criteria: (i) The click was clearly above noise level in at least five microphones. (ii) We excluded beams that were either too wide or too narrow relative to the overall distribution of beam-widths, to exclude the possibility that their abnormal width might be an artifact of sudden noise in one or several channels. To do this, we measured the width of the beam as the angular difference between the right-maximum-slope and the left-maximum-slope of the emission curve, and accepted only clicks with: $30^\circ < \text{beam-width} < 120^\circ$. This resulted in exclusion of ~6% of the clicks (~3% narrow clicks $< 30^\circ$ and ~3% wide clicks $> 120^\circ$). (iii) We excluded all the clicks from the last 250 ms before landing, because these clicks were emitted when the bat was too close to the target (closer than 15 cm on average), and any angular estimates of the bat's angle-to-target would be unreliable at such short distances. This condition corresponded to excluding, on average, the last two click-pairs in each trial. In total, we analyzed here 5,870 sonar clicks from 256 behavioral trials in 6 bats.

Locking criterion: We defined a "locked" click-pair as a pair in which the vector-average direction of its two clicks was $< 30^\circ$ relative to the target. The 30° criterion

was chosen since it corresponds to twice the asymptotic standard deviation of all click-pair vector averages, just before landing (Fig. 2A bottom, yellow lines). We tested two additional criteria for locking threshold (20° and 40°, data not shown), which did not affect the results.

Measuring the Fisher Information (FI): As input to the FI calculation, we used click-intensity coding, as follows: Each recorded click provides us with a set of intensities in a wide range of angles around the target. The clicks were each normalized to have a total power of 1. We used all clicks to estimate the probability density function (PDF) of intensities impinging on different angles relative to the target, as is done with a population of neurons to estimate the PDF of the firing-rate relative to a sensory input (3–5). The direction (relative to the target) of maximal FI therefore represents the direction which is encoded by the PDF that is most different from its surroundings (i.e. most different from the PDF's representing neighboring directions). To smooth the estimated PDF's, we clipped to 0 very low PDF values (<0.005), and then smoothed each PDF with a 3-point Gaussian kernel ($\sigma=1$ pixels). The intensity PDF's were estimated using 10 bins with a bin-width of 0.0025 (normalized intensity units). FI was finally calculated according to (6):

$$I_F(\theta) = \sum_x p(x|\theta) \left[\frac{\partial \log(P(x|\theta))}{\partial \theta} \right]^2$$

Where $I_F(\theta)$ denotes the FI curve as a function of θ , the angle relative to the target; x denotes the click intensity.

Measuring azimuth discriminability: For Fig. 3B, we computed the discriminability d' of a stimulus at azimuth θ from a neighboring stimulus at $\theta+\Delta\theta$, using the following relation (6):

$$d'(\theta) = \Delta\theta\sqrt{I_F(\theta)}$$

Where $\Delta\theta$ is a small change in the location (azimuth) of the stimulus. This calculation assumes a maximum-likelihood based estimator (6). These discriminability values were plotted as the cyan line in Fig. 3B.

Estimating relative changes in detection range: To compare the maximal detection range of a target when the bat uses the beam's peak versus the beam's slope, we utilized the fundamental Radar equation (7):

$$P \propto \frac{A}{R^4} \rightarrow R_{\max} \propto \sqrt[4]{\frac{A}{P_{\det}}}$$

Where A depends on the power of the emitted click, its duration, the sonar cross section of the target, the antenna gain and the atmospheric attenuation; P is the energy of the echo; P_{\det} is the minimal echo energy that the bat can detect; and R is the range to the target. When the direction of the beam relative to the target changes, the variable A changes linearly according to the amount of energy that is directed towards the target. We can then invert the formula and compute R_{\max} = the maximal detection range for the target, which varies as fourth root of the energy that the bat directs toward the target. Since the energy of the maximum-slope of the beam is reduced by 6 dB compared to the peak of the beam, the fourth root calculation shows that there is a reduction of ~16% in maximal detection range when using the slope versus when using the peak of the beam.

Measuring skewness: Skewness of the angular distribution in Fig. 2C (top) was calculated according to:

$$\gamma = \frac{\langle (\theta - \bar{\theta})^3 \rangle}{\langle (\theta - \bar{\theta})^2 \rangle^{3/2}}$$

Where γ denotes the skewness, $\langle \rangle$ denotes the expected value (mean), θ is the angle of the peak relative to target and $\bar{\theta}$ is the average angle. The significance of the skewness was calculated using a t -test, where the standard error s was estimated

according to (8): $s = \sqrt{\frac{6}{n}}$, which is valid in our case since $n > 150$ (ref. 8).

‘Masker experiments’: In these control experiments we positioned the target close to the wall and to the microphones, and placed a large strongly-reflecting styrene board (2.7×1.5 m) closely behind the target, in order to create a detection problem for the bat. To test the accuracy of estimating the beam's direction close to the wall (where a smaller number of microphones pick up the emitted click) we used three controls: (i) We performed calibrations using an ultrasonic speaker pointing in a known direction and compared this direction to the estimated direction as reconstructed from the recording: these directions closely matched. (ii) In our standard experiments (with no reflector on the wall) we examined those trials where the target was positioned relatively close to the wall (as close as 90 cm): we did not find any change of echolocation behavior in those trials compared to trials where the target was distant from the wall (Figs 1-2), i.e., even when flying close to the wall, the bats emitted clicks in the usual alternating manner, Left→Right→Right→Left, and directed the maximum-slope of their clicks towards the target. This suggests that the

peak-directing behavior in Fig. 3C (bottom, black dots) and fig. S6 was elicited by the presence of the reflector (masker), not by the distance from the wall *per se*. (iii) We conducted Monte-Carlo simulations to estimate the minimal distance of the bat from the microphones at which the estimation of the beam's direction is still reliable (note that in this experiment the bat flew very close to the microphones). These simulations were conducted as follows: We positioned a hypothetical bat at random positions in the room, 50–80 cm from the microphones, facing the masker head-on. We used the average call shape (Fig. 3A) in order to produce a simulated emission-beam of the bat at each position, and added Gaussian noise of 0.1 dB similar to the system's noise. We then used the beam-interpolation method described above, and compared the direction of the peak, as estimated using this method, to the real direction of the simulated call that we created. At large distances from the microphones the two directions matched very well, and even at a distance of 50 cm from the microphones, more than 65% of the clicks had an error $< 15^\circ$ – and because the maximum slope of the bat's average beam is at $\sim 30^\circ$, an error of $< 15^\circ$ still allows to tell apart if the bat directs to the target the part of the emission-curve that is closer to the peak versus the part closer to the maximum-slope. We therefore show in Fig. 3C and in fig. S6 only calls that were produced when the bat was > 50 cm from the microphones, i.e. at distances that allowed us to reliably state whether the bat placed on-target a point closer to the peak or a point closer to the maximum-slope of its emission curve. Note that, because in these 'masker experiments' we did not analyze the directional aim of the maximum-slope of the beams (nor did we analyze here the FI) – we only analyzed the direction of the *peak* – a beamwidth criterion was not applied to exclude clicks in these control experiments.

Simulation of olfactory tracking: For the olfactory simulations (Fig. 4) we assumed a schematic odor trail which drops to the sides in a Gaussian manner. We first computed the motion of an organism which follows the *peak* concentration of the odor trail, assuming that the organism can detect a concentration change of 10% of the peak, with an average error of 3% (i.e. detection threshold was set randomly to a value within the range $10 \pm 3\%$, mean \pm s.d.; Fig. 4, gray line). The 3% error is meant to represent both errors in the accuracy of the biological sensory detector as well as possible local fluctuations in the odor concentration. Such a peak-following strategy is typically assumed for odor-trail following (9, 10). We then computed the motion of the same organism when using a strategy similar to our bats – i.e., following the maximum *slope* of the odorant concentration – and assuming the same threshold of 10% for detecting concentration changes, and the same error of 3% (Fig. 4, black line). The trajectory jitter in the slope-following case (black line) is much smaller, making the motion smoother and more accurate.

Supplementary Text

Sound production mechanism of the left/right clicks: The mechanism used by the bats to direct their clicks sideways is not entirely clear (11, 12). There are three possibilities: (i) Head motion, (ii) lip motion, (iii) tongue motion. We examined option (i) by both regular and high-speed video cameras, as well as by visual observations, but none of these revealed any motion of the head between the emissions of the two clicks within a pair. Further, such a large angular movement of

the head is mechanically highly unlikely within such a short time interval (20 ms).

(ii) High-speed videos revealed that the bats open the entire mouth to a narrow slit during the emission of both of the clicks of a single click-pair, without any obvious lip motion within the 20-ms between the clicks. We therefore believe that (iii) *tongue motion* is the most likely mechanism of the Left→Right directioning of the sonar beam in space: that is, the motion of the tongue laterally inside the mouth from left to right would steer the sonar beam in space in the opposite direction, from right to left; and vice versa in the next click-pair. However, to confirm this possibility would require an entirely different method that allows high-speed imaging of tongue movements *inside* the mouth.

References

1. K. Ghose, C. F. Moss, *J. Acoust. Soc. Am.* **114**, 1120 (2003).
2. K. Ghose, C. F. Moss, *J. Neurosci.* **26**, 1704 (2006).
3. N. S. Harper, D. McAlpine, *Nature* **430**, 682 (2004).
4. I. Dean, N. S. Harper, D. McAlpine, *Nat. Neurosci.* **8**, 1684 (2005).
5. N. Gordon, T. M. Shackleton, A. R. Palmer, I. Nelken, *J. Neurosci. Meth.* **169**, 391 (2008).
6. P. Dayan, L. F. Abbott, *Theoretical Neuroscience* (MIT Press, Cambridge, 2001).
7. M. Skolnik, *Introduction to Radar Systems*, 3rd ed. (Mcgraw-Hill, New York, 2002).
8. R. R. Sokal, F. J. Rohlf, *Biometry: The Principles and Practices of Statistics in Biological Research*, 3rd ed. (Freeman, New York, 2001).
9. I. D. Couzin, N. R. Franks, *Proc. Biol. Sci.* **270**, 139 (2003).
10. J. Porter *et al.*, *Nat. Neurosci.* **10**, 27 (2007).
11. R. A. Holland, D. A. Waters, J. M. Rayner, *J. Exp. Biol.* **207**, 4361 (2004).
12. E. Kulzer, *Z. Vergl. Physiol.* **43**, 231 (1960).

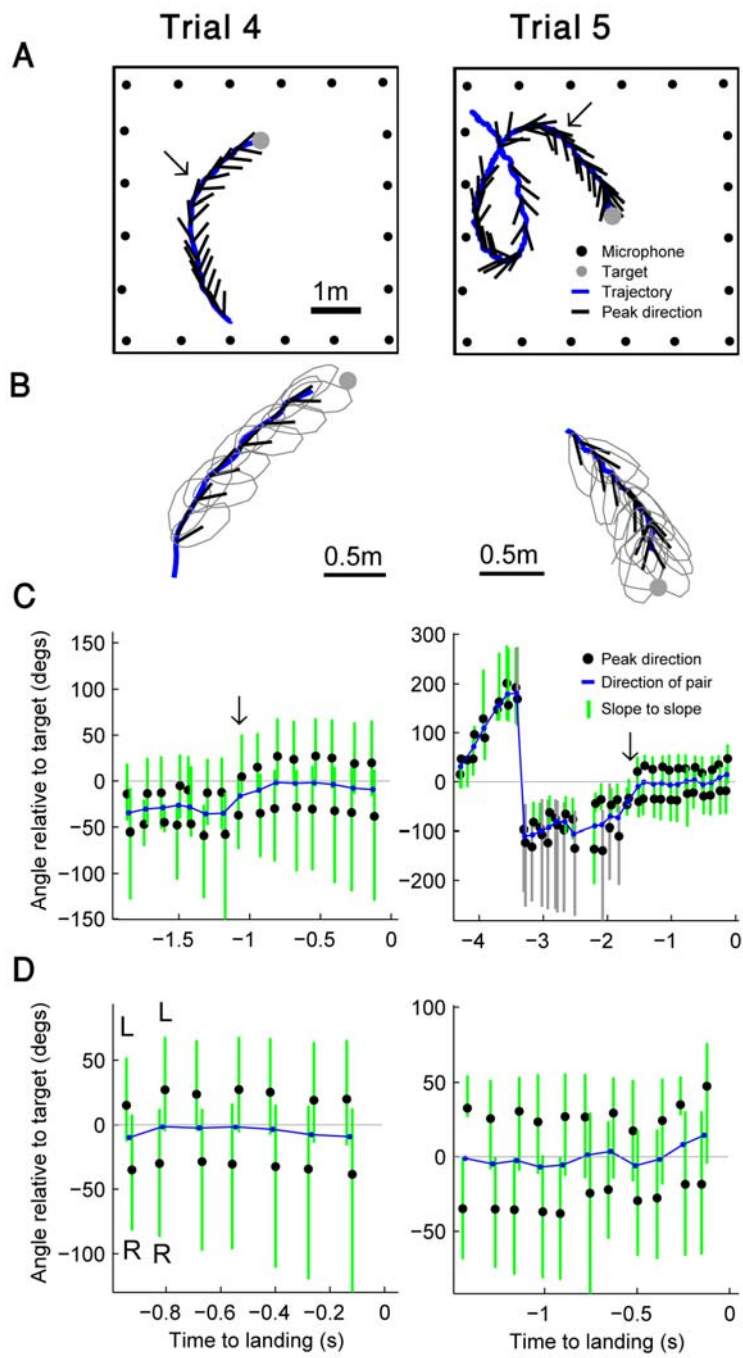


fig. S1. Examples of flight and echolocation behavior. Notations are as in Fig. 1.

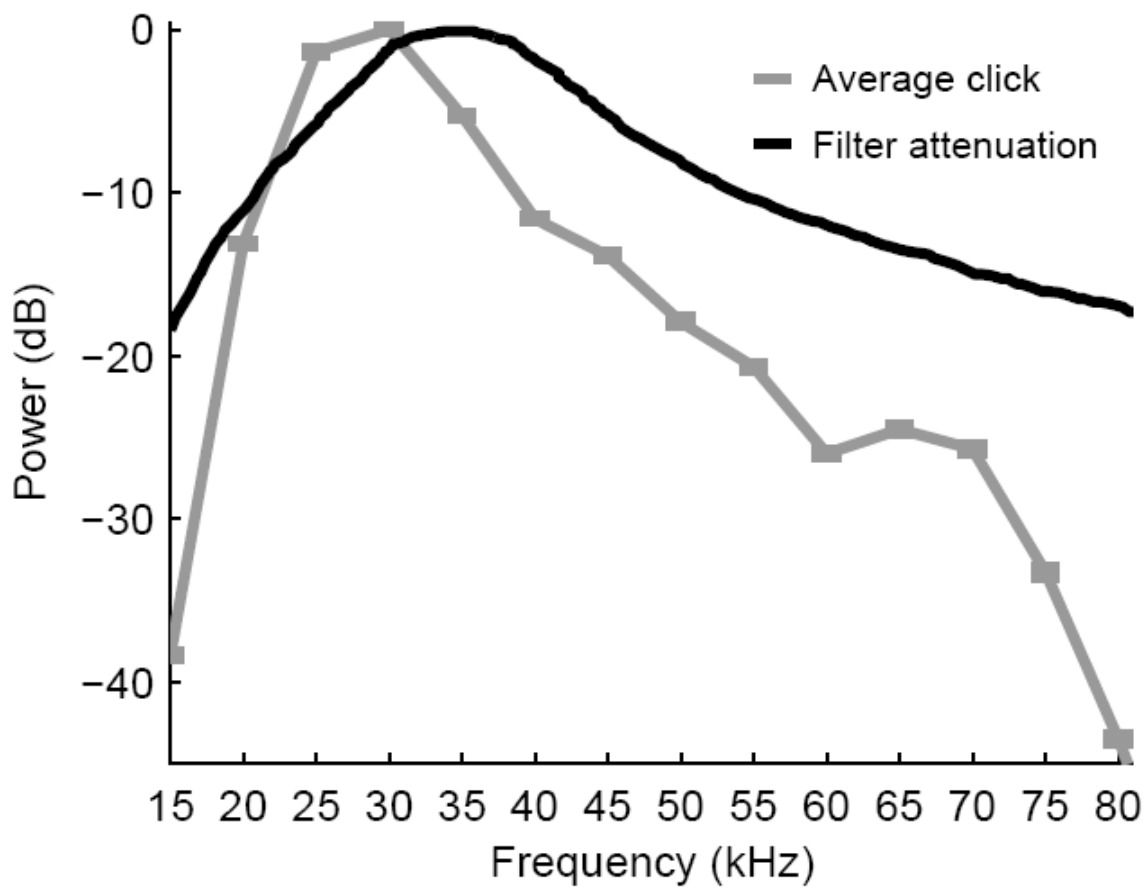


fig. S2. Spectrum of sonar click matches the filtering characteristics of the audio recording system. The system has good sensitivity in the frequency range where the clicks have high energy (20–45 kHz). Click spectrum is based on 80 clicks recorded with a wideband microphone.

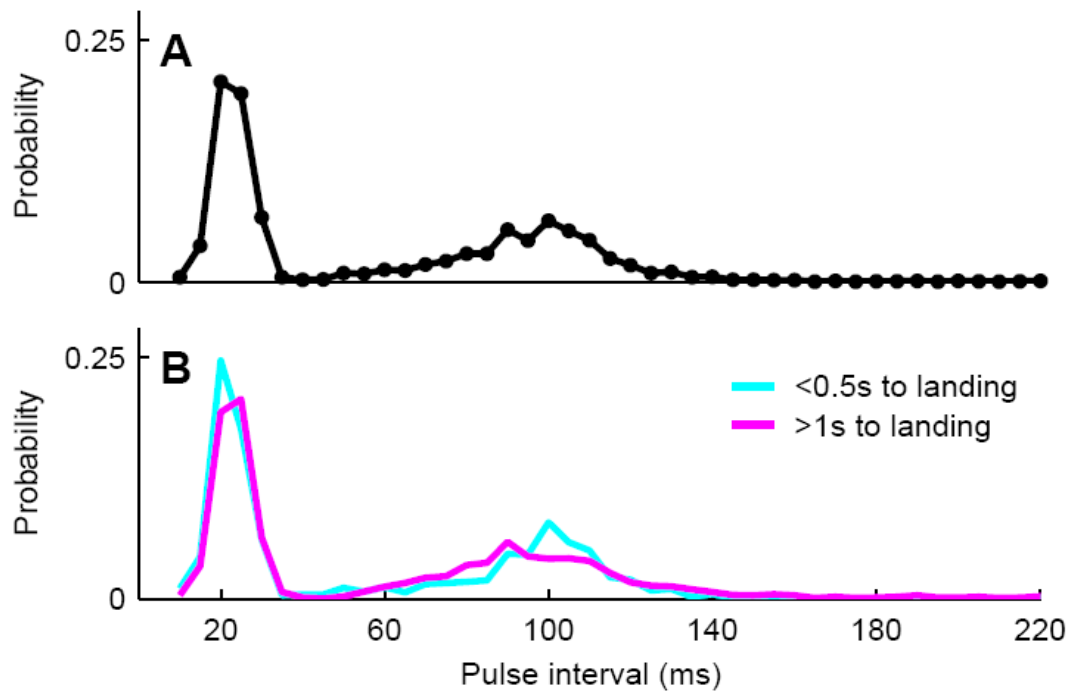


fig. S3. Distribution of time intervals between consecutive sonar clicks (pulse-interval histogram). Data from all bats. **(A)** The distribution of pulse intervals pooled for all parts of the flight. The clear bi-modal distribution demonstrates that the bats used intra-pair intervals of 20-25 ms and inter-pair intervals of 90-100 ms. **(B)** A finer analysis of the distribution of intra-pair time intervals in different time epochs prior to landing reveals that, in the last 0.5 seconds, the bats tended to reduce the intra-pair interval to ~20 ms and increase the inter-pair intervals to ~100 ms – thus maintaining the overall cycle duration at ~120 ms. (We divided the data here based on time-epochs and not based on distance from target, because during the flight the bats changed their distance from the target in a complex manner that was not necessarily related to the approach, e.g., circling the target.) The reduction of the intra-pair click interval towards the end of the approach (cyan) strengthens the hypothesis that the bats might compare the energy reflected from two intra-pair clicks in order to determine whether they are flying straight towards the target (see main text): A shorter time-interval between clicks makes it easier for the bat to compare the energy reflected from the target across the two clicks. This reduction in intra-pair click interval could also be a result of the shorter echo-delay at the shorter ranges.

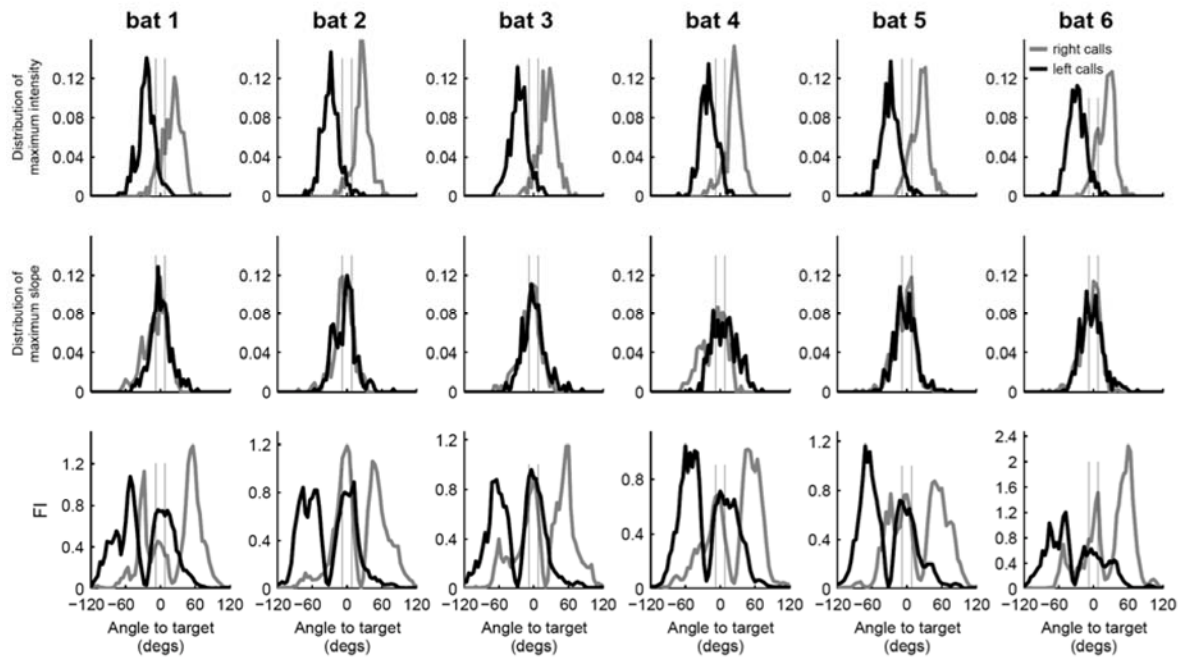


fig. S4. Distributions of click parameters and Fisher Information (FI) in the locked phase for all six bats. Top: distribution of the angles of the emission curve's peak relative to the target. Middle: distribution of the angles of emission curve's maximum-slope relative to the target. Bottom: the FI for different angles relative to the target.

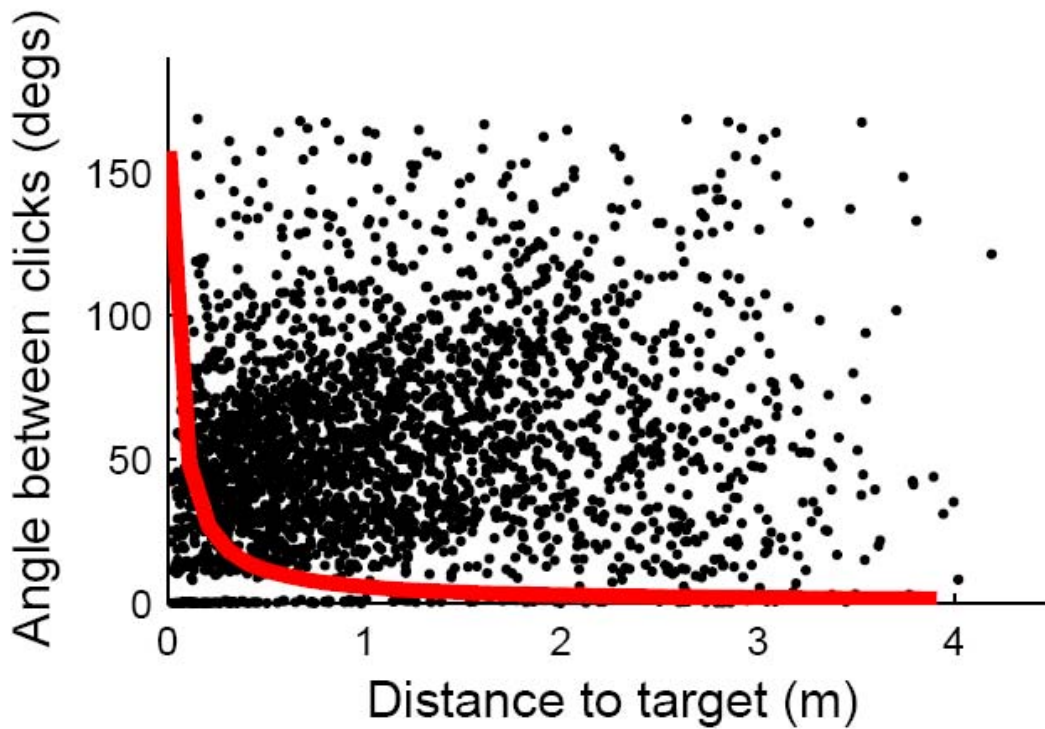


fig S5. Scatter plot of the angle between the two beams of a click-pair (i.e. the angle between the peak directions of the two consecutive clicks) as function of the bat's distance to target. Data from all bats. The red line shows the theoretically expected angle if the bats were pointing the peak of their beams towards the edges of the target (a 10-cm diameter sphere); the red line varies according to: $Angle = 2 \times \tan^{-1}(R/D)$, where $R = 5$ cm is the radius of the target, and D the distance to the target. The actual data (black dots) clearly deviate dramatically from the red line, suggesting that the bats did *not* point the peak of their beams onto the edges of the target. Further, as the red line shows, we would generally expect negative correlation between angle and distance (i.e. beams should open up as the bat is approaching the target); however, calculation of the correlation coefficient of the scatterplot shows *positive* correlation ($r = 0.192$), which is again inconsistent with the notion that the bats were pointing the beams' peaks towards the edges. In fact, this correlation r is quite low, which is consistent with the notion that the bats kept the *maximum slope* of the beam on the *center* of the target.

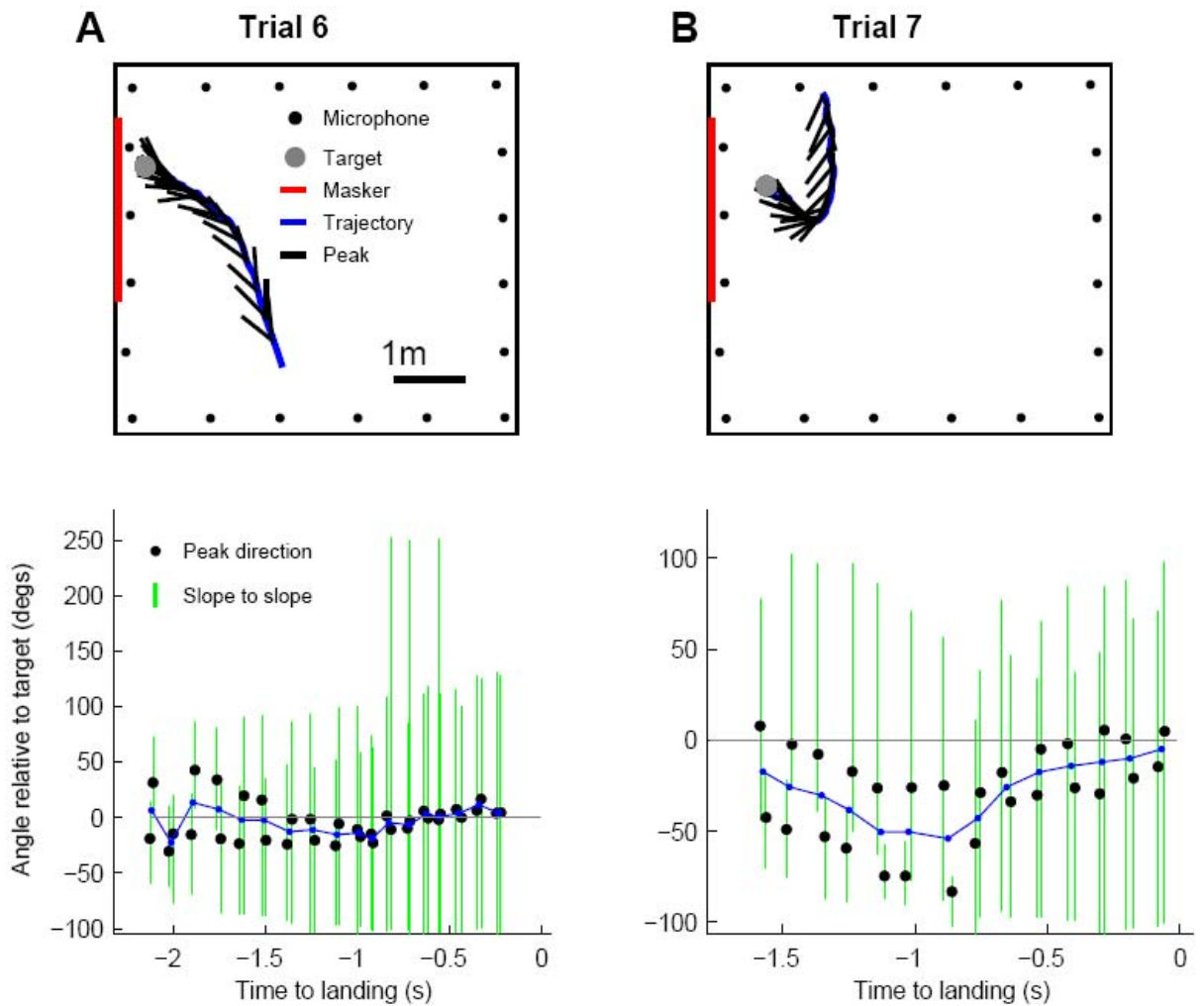


fig. S6. Additional examples from the experiment in which a strong reflector (masker) was placed behind the target. (A-B) Two examples of trials (trajectories and echolocation behavior) taken from bats #2 and #5, respectively; same notations as in Fig. 3C. These examples demonstrate the transition between a strategy of Left→Right→Right→Left directional alternation, where the bat positions the maximum slope on-target, to another behavioral strategy whereby the bat positions onto the target a point close to the beam's *peak*. The behavioral transition occurs ~1.3 seconds before landing in Trial 6 and ~0.8 seconds before landing in Trial 7 (see bottom panels, black dots). These examples, similarly to Fig. 3C, demonstrate the bat's behavioral flexibility.

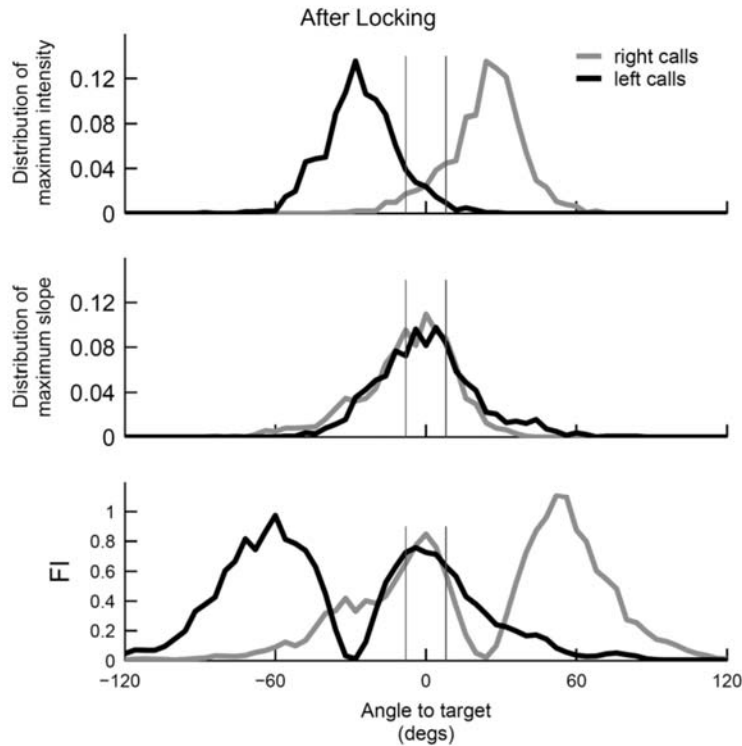


fig. S7. Distributions of click parameters and FI for clicks produced during horizontal flight at the height of the microphones. Because we used a planar array of microphones, we could only estimate a cross-section through the three-dimensional beam. Such a cross-section reliably reflects the emission curve of the beam if: (i) the horizontal beam shape is preserved along the vertical axis, and (ii) The bat's head is not tilted relative to the horizon. To test the effect of this potential bias on our data, we conducted the control analysis presented here, where we included only clicks in which the bat was flying horizontally and at the height of the microphones. To do this, we excluded clicks that were produced when the bat was flying upwards or downwards with a high vertical velocity (higher than the mean) and/or when the bat was more than 30 cm higher or lower than the microphones. Because the bats did *not* tend to bank during flights, these clicks (N = 2,841 clicks, 48% of total clicks) represent a subset of the clicks in which we could estimate a cross-section that is close to an ideal horizontal cross-section through the beam. The results of this analysis are shown here, and are very similar to the analysis of the full data (compare to Fig. 2C, notations here are the same): This suggests that the beam's cross-section, as recorded by the horizontal 20-microphone array, represents well the true central cross-section through the beam.

Supplementary Movie:

Supplementary Movie: Example trial. (Right window) Raw video from one camera, slowed down 8× times. (Left window) Top-view of the flight trajectory and the echolocation behavior. Gray circle, target. Black circles, microphones. Blue line, flight trajectory. Magenta, spatial pattern of sonar beam (emission curve) in polar coordinates (dB). Black lines, direction of the clicks' peak intensity.